Simultaneous Visualization of Induction and Reaction Zones by Planar Laser Induced Fluorescence in Hydrogen Detonations

Samir B. Rojas Chavez, Karl P. Chatelain, Mhedine Alicherif, Deanna A. Lacoste

Mechanical Engineering Program, Physical Science and Engineering Division, King Abdullah University of Science and Technology (KAUST), Thuwal, 23955-6900, Saudi Arabia

Clean Combustion Research Center (CCRC), King Abdullah University of Science and Technology

1 Introduction

Detonation waves have been studied for more than seventy years [1], using techniques such as schlieren or shadowgraph, and $CH^\star$ or $OH^\star$ chemiluminescence for visualization of the shock and reaction zone dynamics [2]. However, these techniques are limited in achieving quantitative measurements due to their light-integrated information and the three-dimensional (3D) nature of detonations. For information with negligible light integration, planar laser-induced fluorescence (PLIF) can be used, providing narrow depth-of-field information of typically $\sim$300 µm.

Planar laser-induced fluorescence has been used to characterize the combustion phenomena in both canonical flame configurations and engines, enabling measurements of temperature and number density of different molecules [3]. Meanwhile, most diagnostic techniques for detonations have only provided qualitative data. The OH-PLIF technique has been used to visualize the reaction zone of detonations in several studies [4–8], revealing characteristic structures and assessing the effects of combustor geometry on the reaction front [9, 10]. Temperature measurements, at equilibrium conditions, have also been conducted using the two-color OH-PLIF technique [11].

Recently, a proof-of-concept of induction zone length measurements was carried out for H_2-air detonations using laser-induced fluorescence of nitric oxide (NO-LIF) [12, 13], enabling one-dimensional (1D) visualization of the induction zone. Note that the shock structure (i.e., Mach stem and incident shock) was not identified in the detonation front. Simultaneous visualization of the induction and reaction zones would be useful to better understand the relationship between the detonation front and exothermic reactions after the von Neumann (vN) state. While such combined diagnostics typically require two dye laser systems, a recent study demonstrated the use of a single dye laser for simultaneous NO-PLIF and OH-PLIF imaging in H_2 jet flames by employing both the frequency-mixed and residual beams from the mixing unit of a dye laser [14]. In this context, the present study aims to visualize simultaneously, with a single dye laser, the induction and reaction front by NO-PLIF and OH-PLIF on H_2 detonation, respectively.

2 Experimental Setup and Methodology

2.1 Diagnostics

The laser system used in our previous NO-LIF study [13] was employed with some modifications that are explained in details in [14]. In short, the Pellin-Broca prism was adjusted to enable all the beams (i.e., at 283 nm, 566 nm, and 225 nm) to exit the frequency and mixing unit. The beam with 566-nm

Correspondence to: samirboset.rojaschavez@kaust.edu.sa

wavelength was blocked with an iris diaphragm after the output of the laser to isolate both the 283-nm and 225-nm beams. Consequently, the two beams, near 225 nm and 283 nm, were both controlled by a single laser pulse and a single angle of the dye laser's grating. Based on the recommendations from [14], simultaneous excitation of OH and NO can be achieved near 285.013 nm and 224.814 nm, respectively, for a specific grating angle. For OH-PLIF, the excitation wavelength at 285.013 nm corresponds to the excitation of the P2(6) and P12(6) transition lines in the (1,0) vibrational band. For NO-PLIF, the excitation wavelength at 224.814 nm corresponds to the excitation of the five transition lines P1(40), Q2(35), R1(26), Q12(35), and R21(26) in the (0,0) vibrational band.

The beams for NO-PLIF and OH-PLIF were separated to follow different optical paths, allowing a short delay of 30 ns at their arrival in the measurement area. This strategy was implemented to allow a short temporal delay between the two PLIF images, improving their quality. Both beams were merged with a custom dichroic mirror (see [15]). The merged beams were reshaped into laser sheets of 12-mm height and 300-μm thickness by employing cylindrical and spherical lenses of -400-mm and +1000-mm focal length, respectively. The laser sheet had a frontal orientation with respect to the detonation front (see [15]). The energy per pulse, inside the test rig, was 1.8 mJ for both laser sheets.

The collection system consisted of two intensified-CCD cameras (PI-MAX4) enhanced in the UV region. Both cameras were equipped with UV lenses (Cerco, f = 100 mm, f/2.8), and were placed in front of the optical access (i.e., UV grade fused silica window) with a collection angle of 75°. A ninety-degree collection angle was not possible due to geometrical constraints of the setup. A long-pass filter (Semrock LP02-224R) was installed in front of the NO-PLIF camera to collect the light above $\approx$ 230 nm, and a short-pass filter (Asahi spectra ZUS0265) was added to block the light above 265 nm. This filter arrangement was selected to collect only NO-LIF signal on the NO camera and to avoid both OH-PLIF and OH* signal contamination. The OH-PLIF camera was equipped with a bandpass filter (LaVision, 110760) centered at 320 nm to collect the OH-LIF signal in the (0,0) band. The optical arrangement allowed a 12-µm spatial resolution. A 25-ns exposure time was used on both cameras to maximize the LIF signal and mitigate chemiluminescence interference.

Simultaneous excitation scans of OH-PLIF and NO-PLIF were performed to determine the excitation for both LIF processes. The obtained scans were similar to those obtained in [14]. The scans were carried out on a Bunsen burner of 1.4-mm diameter, with a stoichiometric laminar H_2-air flame at atmospheric conditions and seeded with 2000 ppm of NO. The burner was aligned with the plane of the field of view (i.e., inside the detonation setup) established to visualize the PLIF images for detonations. After the scans were conducted, the burner was removed and the detonation setup was closed to run detonation experiments.

2.2 Experimental setup

The Optical Detonation Duct (ODD), described in [8] was employed for this study. The ODD is a 3.5-m long rectangular duct with a 170 × 40 mm^2 cross-section and equipped with large optical accesses for laser diagnostics. At the end wall of the ODD, a quartz window of 80 × 13 mm^2 is used as the entrance window for the laser sheet. A stoichiometric mixture of hydrogen diluted with argon ($2H_2$-O_2-3.76Ar) at $P_1 = 20$ kPa and $T_1 = 293$ K initial condition was tested. Finally, 1900 ppm of NO were added to the mixtures to enable the NO-PLIF measurements. This concentration was chosen as a good compromise between a good signal-to-noise ratio and a negligible effect on the detonation properties (i.e., detonation structure and propagation speed), as discussed in [13, 16]. The experimental procedure detailed in [8] was followed in the present study.

2.3 Post-processing Procedure

The raw images were corrected following this procedure. First, the background was subtracted to account for the camera noise. Second, the coordinates of the OH-PLIF images were corrected with respect to the NO-PLIF images. Third, both PLIF images were denoised using a guided filtered approach [17]. Finally, each image was normalized with respect to its maximum intensity.

3 Results

Figure 1 shows a typical result obtained from the simultaneous OH-PLIF and NO-PLIF imaging. Figure 1a corresponds to OH-PLIF, in red, and Fig. 1b corresponds to the NO-PLIF, in blue. The detonation is traveling from left to right, and the laser sheet propagates opposite to the detonation front. Two structures are identified and annotated in both images: the Mach Stem (MS) and Incident Shock (IS). As discussed in [13], for an excitation at 225.120 nm, the fluorescence of NO mainly follows the number density of NO. Despite a slightly different laser excitation wavelength, a similar LIF profile evolution was also obtained in the present study. Thus, the signal increases at the shock location and reaches its maximum intensity at the von Neumann state (vN). The signal remains in a quasi-plateau and decays in the burned gases. The OH-PLIF image marks the exothermic part in the detonation front with a similar LIF signal dynamic as obtained in the OH-LIF images of Pintgen [7] and Austin [5] with a 284-nm excitation wavelength. Both observations are in agreement with the estimated LIF profile evolution from spectroscopic tools (e.g., KAT-LIF or LIFBASE). Note that OH and NO molecules are excited simultaneously for the first time in detonation conditions with a single laser system, which significantly reduces the cost of the dual-diagnostic. This simultaneous diagnostic enables two-dimensional visualization of both the induction and exothermic zones at different locations within the detonation front.

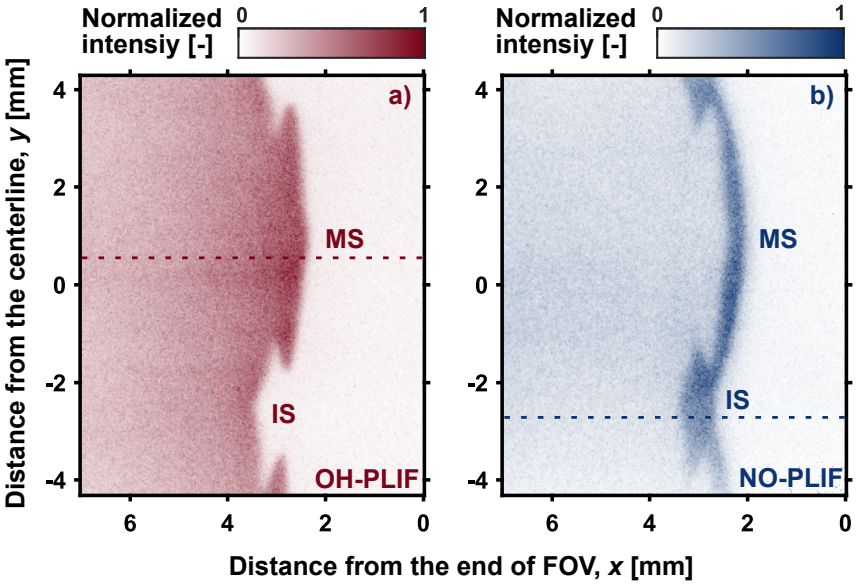

Figure 1: Example of simultaneous OH-PLIF and NO-PLIF images obtained for a $2H_2$-O_2-3.76Ar detonation at $P_0 = 20$ kPa and $T_0 = 293$ K initial condition. OH-PLIF intensity is represented in red color in a). NO-PLIF intensity is represented in blue color in b). MS and IS stand for Mach Stem and Incident Shock, respectively.

Figure 2 shows one-dimensional profiles obtain from Fig.1. The profiles of Fig.2a are for the Mach Stem structure located at $y = 0.6$ mm. Figure 2b shows the profiles of the Incident shock at $y = -2.7$ mm.

All profiles were obtained by averaging 240 μm (20 pixels) in the y axis and normalized with respect to their own maximum intensity. Thus, the curvature and non-orthogonality effects play a negligible role in the evolution of the profiles. As expected, the NO-LIF signal, depicting the induction zone, rise earlier compared to the OH-LIF signal for both structures. Later, the NO-LIF signal decreases while the OH-LIF signal increase in the exothermic part. Note that for both IS and MS structures, the OH-LIF signal starts rising near the same location that NO-LIF start decreasing: at $x = 2.3$ mm for MS and $x = 3.2$ mm for IS. Also, note that the OH-LIF signal reaches its maximum value at the time that the NO-LIF signal reaches the plateau in the burned gases, at $x = 2.56$ mm for MS, and at $x = 3.57$ mm in the IS. In addition, the distance between the two LIF maxima appears as a good indicator of the coupling between the shock wave and the reaction front (i.e., exothermic pulse).

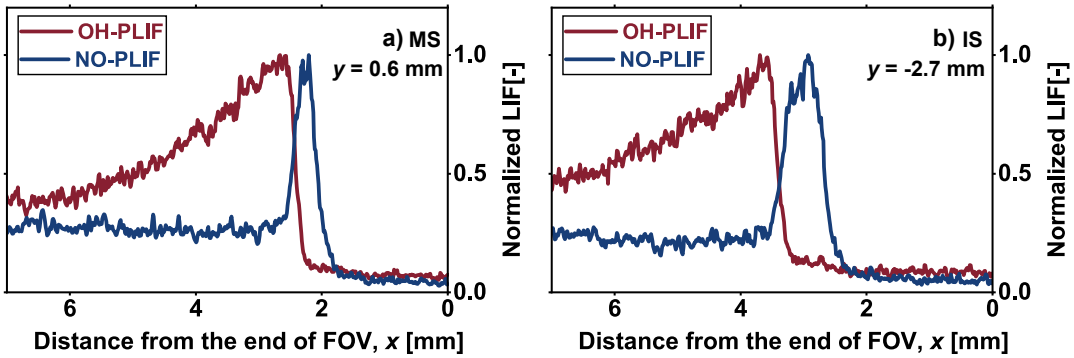

Figure 2: One-dimensional profiles extracted from the dotted lines of the OH-PLIF and NO-PLIF images. The profiles were obtained averaging 240 μm in the y axis. (a) Profiles corresponding to the Mach Stem (MS) located at $y = 0.6$ mm. (b) Profiles extracted from the Incident shock (IS) located at $y = -2.7$ mm

Figure 3 shows a different stage of the detonation cycle compared to Fig. 1. It captures the initiation of a new detonation cell at $y = 0$ mm. Two MS are identified at the top and bottom of both OH-PLIF and NO-PLIF figures. Both are at the end of the first half of the cycle, i.e., near the transition to IS. In the space between these MS, postshock gases are confined, as shown by blue shades in Fig. 3b, and a blank area in Fig 3a, also known as ignition kernels [18]. This feature is reminiscent of the previous keystone structure at the end of the cycle. At this moment, a new cell is formed, which appear as a jetting-like shape in the OH-PLIF figure. Notably, the NO-PLIF image does not a reveal signal ahead of the reaction zone, which can be expected in the y_1 location. This suggests extreme thermodynamic conditions that could lead to rapid ignition and a small induction length beyond the spatial resolution. This technique provides a robust visualization of the dynamics during the cellular cycle, including extreme events such as the one shown in Fig. 3. Consequently, these data can offer insights into the controlling mechanism of the cellular nature of detonations.

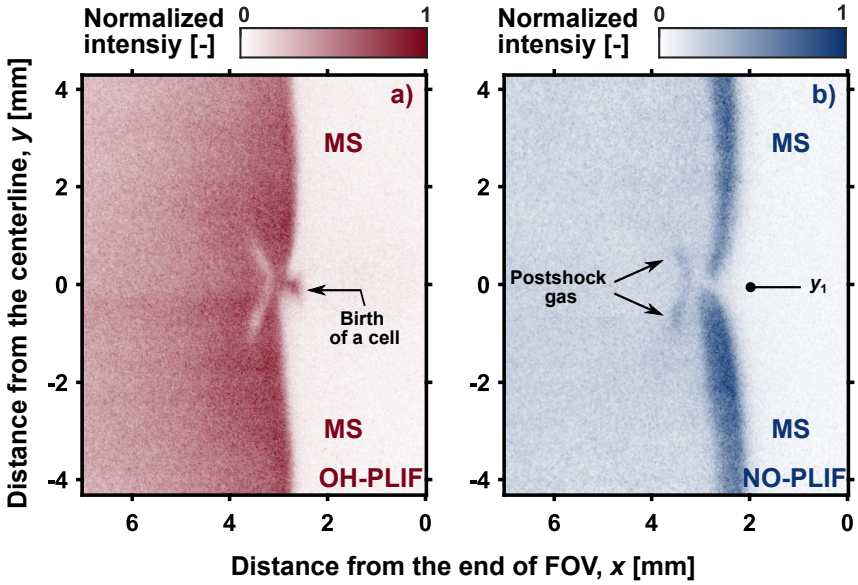

Figure 3: Simultaneous OH-PLIF and NO-PLIF images obtained at the birth of a new cell. OH-PLIF intensity is represented in red color in a). NO-PLIF intensity is represented in blue color in b). MS and IS stand for Mach Stem and Incident Shock, respectively. y_1 represents the expected location of the induction zone.

4 Conclusions

Simultaneous visualization of the induction zone and reaction front was performed by using the NO-PLIF and OH-PLIF technique in $2H_2$-O_2-3.76Ar detonations, at $P_1 = 20\,\text{kPa}$ and $T_1 = 293\,\text{K}$ initial conditions. The main conclusions are:

- Simultaneous OH-PLIF and NO-PLIF can be performed using only one dye laser for detonation conditions. The use of the residual beam, created by the mixing process, and the mixed-beam enables simultaneous single-shot imaging of the detonation front.
- The selected excitation schemes, i.e, 285.013 nm for OH-PLIF and 224.814 nm for NO-PLIF, showed similar LIF intensity dynamics compared to other excitation schemes provided in the literature.
- The combined one-dimensional fluorescence profiles revealed the location of the shock, the induction zone, and the reaction front for both mach stem and incident shock.

Future studies will assess the quantitative potential of using both PLIF signals. Furthermore, this technique can be used to characterize better the shock-reaction coupling and might help to understand the presence of unburned pockets for unstable mixtures.

Acknowledgments

This work has been supported by the King Abdullah University of Science and Technology through the baseline fund BAS/1/1396-01-01.

References

[1] J. H. S. Lee, *The Detonation Phenomenon*. Cambridge: Cambridge University Press, 2008.

[2] M. D. Frederick, R. M. Gejji, J. E. Shepherd, and C. D. Slabaugh, "Time-resolved imaging of the cellular structure of methane and natural gas detonations," *Shock Waves*, pp. 1–15, 2022.

[3] T. F. Guiberti, Y. Krishna, W. R. Boyette, C. Yang, W. L. Roberts, and G. Magnotti, "Single-shot imaging of major species and OH mole fractions and temperature in non-premixed H_2/N_2 flames at elevated pressure," *Proc. Combust. Inst.*, vol. 38, no. 1, pp. 1647–1655, 2021.

[4] J. M. Austin, F. Pintgen, and J. E. Shepherd, "Reaction zones in highly unstable detonations," *Proc. Combust. Inst.*, vol. 30, no. 2, pp. 1849–1857, 2005.

[5] J. Austin, "The role of instability in gaseous detonation," Ph.D. dissertation, California Institute of Technology, 2003.

[6] J. E. Shepherd, "Detonation in gases," *Proc. Combust. Inst.*, vol. 32, pp. 83–98, 2009.

[7] F. Pintgen, C. A. Eckett, J. M. Austin, and J. E. Shepherd, "Direct observations of reaction zone structure in propagating detonations," *Combust. Flame*, vol. 133, no. 3, pp. 211–229, 2003.

[8] S. B. Rojas Chavez, K. P. Chatelain, T. F. Guiberti, R. Mével, and D. A. Lacoste, "Effect of the excitation line on hydroxyl radical imaging by laser induced fluorescence in hydrogen detonations," *Combust. Flame*, vol. 229, p. 111399, 2021.

[9] C. A. Fugger, P. S. Hsu, N. Jiang, S. Roy, M. Slipchenko, V. Athmanathan, A. Webb, J. Fisher, and T. R. Meyer, "Megahertz OH-PLIF imaging in a rotating detonation engine," in *AIAA Scitech 2021 Forum*, 2021, p. 555.

[10] P. S. Hsu, M. N. Slipchenko, N. Jiang, C. A. Fugger, A. M. Webb, V. Athmanathan, T. R. Meyer, and S. Roy, "Megahertz-rate OH planar laser-induced fluorescence imaging in a rotating detonation combustor," *Opt. Lett.*, vol. 45, no. 20, pp. 5776–5779, oct 2020.

[11] S. W. Grib, C. A. Fugger, P. S. Hsu, N. Jiang, S. Roy, and S. A. Schumaker, "Two-dimensional temperature in a detonation channel using two-color OH planar laser-induced fluorescence thermometry," *Combust. Flame*, vol. 228, pp. 259–276, 2021.

[12] K. P. Chatelain, S. B. Rojas Chavez, J. Vargas, and D. A. Lacoste, "Towards Laser-Induced Fluorescence of Nitric Oxide in Detonation," *28th ICDERS*, 2022.

[13] S. B. Rojas Chavez, K. P. Chatelain, and D. A. Lacoste, "Induction zone length measurements by laser-induced fluorescence of nitric oxide in hydrogen-air detonations," *Proc. Combust. Inst.*, 2022.

[14] K. P. Chatelain, G. Wang, and T. F. Guiberti, "Simultaneous planar laser-induced fluorescence of nitric oxide and hydroxyl radical with a single dye laser," *Int. J. Hydrog. Energy.*, 2023, (Under review).

[15] K. P. Chatelain, R. Mével, J. Melguizo-Gavilanes, A. Chinnayya, S. Xu, and D. A. Lacoste, "Effect of incident laser sheet orientation on the OH-PLIF imaging of detonations," *Shock Waves*, vol. 30, no. 7, pp. 689–702, 2020.

[16] K. P. Chatelain, M. Alicherif, S. B. Rojas Chavez, and D. A. Lacoste, *Nitric oxide sensitization of hydrogen detonations*. National Harbor, Maryland: AIAA Scitech 2023 Forum, 2023, AIAA 2023-1877.

[17] K. He, J. Sun, and X. Tang, "Guided image filtering," *IEEE transactions on pattern analysis and machine intelligence*, vol. 35, no. 6, pp. 1397–1409, 2012.

[18] J. Crane, J. T. Lipkowicz, X. Shi, I. Wlokas, A. M. Kempf, and H. Wang, "Three-dimensional detonation structure and its response to confinement," *Proceedings of the Combustion Institute*, 2022.